JGR Earth Surface

RESEARCH ARTICLE
10.1029/2018JF004785

Infrasound Array Analysis of Debris Flow Activity and Implication for Early Warning

E. Marchetti[1], F. Walter[2], G. Barfucci[1], R. Genco[1], M. Wenner[2], M. Ripepe[1], B. McArdell[3], and C. Price[4]

[1]Department of Earth Sciences, University of Firenze, Firenze, Italy, [2]Laboratory of Hydraulics, Hydrology and Glaciology, ETH, Zürich, Switzerland, [3]WSL, Swiss Federal Institute for Forest, Snow and Landscape Research, Birmensdorf, Switzerland, [4]Department of Geosciences, Tel Aviv University, Tel Aviv, Israel

Key Points:
- Infrasound array analysis shows that debris flows can be modeled as an extended source of infrasound with variable phase
- Seismic and infrasound spectra of debris flows at Illgraben are decoupled and suggest two different mechanisms of energy radiation
- When sharp topography is present, infrasound arrays can be used as an efficient early warning systems for debris flows remotely

Correspondence to:
E. Marchetti,
emanuele.marchetti@unifi.it

Citation:
Marchetti, E., Walter, F., Barfucci, G., Genco, R., Wenner, M., Ripepe, M., et al. (2019). Infrasound array analysis of debris flow activity and implication for early warning. *Journal of Geophysical Research: Earth Surface*, *124*, 567–587. https://doi.org/10.1029/2018JF004785

Received 19 JUN 2018
Accepted 26 JAN 2019
Accepted article online 2 FEB 2019
Published online 14 FEB 2019

Abstract Debris flows constitute a severe natural hazard and studies are performed to investigate triggering mechanisms and to identify and evaluate early warning systems. We present a seismoacoustic analysis of debris flow activity at Illgraben, Switzerland, with infrasound data collected with a small aperture array. Events are recorded as emergent signals of long duration, with seismic and infrasound amplitudes scaling with the flow discharge. The spectral content is stable and peaking at 8 Hz for the seismic and at 5 Hz for the infrasound that suggests two separate processes of elastic energy radiation, most likely bed-load transport for the seismic and waves at the free surface for the infrasound. Although amplitude and frequency content of the infrasound signal are well within the processing limits, most of the signal is not showing any correlation among the array elements. We suggest that this is a consequence of the contribution of multiple sources of infrasound acting with variable amplitude and phase along the surface of the debris flow. At Illgraben, coherent infrasound is recorded only from fixed sources, corresponding to check dams within the channel. Here infrasound radiation is increased and the dams turn into predominant sources of energy. This allows to unambiguously identify the occurrence of debris flow at Illgraben with the infrasound array, from a remote and safe position and with a timing that is similar to the early warning system based on in-channel sensors. This clearly shows how infrasound arrays could be used as an efficient early warning systems.

Plain Language Summary Debris flows constitute a severe natural hazard in alpine environments, and studies are currently performed to investigate triggering mechanisms and to identify and evaluate early warning systems. We present a seismoacoustic analysis of debris flow activity at Illgraben, Switzerland, with infrasound data collected for the first time with an array of infrasound sensors deployed outside the channel in a safe position. This seimoacoustic experiment is providing interesting constraints on the mutual radiation of energy in the ground and in the atmosphere by the flow. Moreover, the use of the infrasound antenna allowed for the first time to carefully analyze the mechanism of infrasound radiation that we model as an extended source of energy with variable phase. Moreover, the array is able to detect the debris flow when it crosses dams or topography steps, even if this occurs at large distance (>2 km) and despite not being visible from the recording site. For the specific case of Illgraben, this allows to unambiguously identifying the occurrence of debris flow with a timing that is similar to the early warning system based on in-channel sensors. This clearly shows how infrasound arrays could be used as new early warning systems for debris flow activity.

1. Introduction

Debris flows are mobilized water/sediment mixtures in steep mountain torrents and constitute a severe natural hazard for downstream communities. Glacier lake outburst floods, natural dam failures, or landslides may initiate debris flows in a much less predictable way than more common precipitation-triggered events. Debris flow events have been investigated extensively through seismic and acoustic observations (see, e.g., Allstadt et al., 2018; Arattano & Marchi, 2005; Burtin et al., 2008; Kean et al., 2015; Kogelnig et al., 2014; Lai et al., 2018; Schimmel et al., 2018; Walter et al., 2017), both to investigate the process and evaluate the potentials for remote monitoring.

Theoretical and experimental studies of seismic energy radiation by debris flow suggest a strong analogy with rivers (Kean et al., 2015; Lai et al., 2018), with seismic energy most likely radiated by the collisions within the boulder snout. Lai et al. (2018) developed a mechanistic physical model for seismic energy radiation by debris flow starting from the bed load transport model proposed for rivers (Burtin et al., 2008; Gimbert et al., 2014; Tsai et al., 2012) and showed how frequency depends only on the source-to-receiver distance, while amplitude of seismic ground shaking is proportional to boulder size and flow velocity as well as boulder snout extension. This was confirmed by direct seismic observations of the 9 January 2018 Montecito debris flow (Lai et al., 2018) that also suggested the existence of additional sources radiating energy within different frequency bands, possibly related to water flow interaction with channel bed and banks and standing waves (Schmandt et al., 2013).

Among the others, waves at the water free surface are considered the most efficient mechanism of infrasound energy radiation by rivers (Schmandt et al., 2013). However, experimental observation showed that infrasound is mostly generated in fixed position, whenever waterfalls are present (Kudo, 1993). In particular, Feng et al. (2014) suggest that infrasound is produced at dams for water falling into the absorption pool that triggers waves radiating infrasound as a dipole source. Therefore, it is expected to have multiple sources of infrasound from rivers according to flow dynamics and channel geometry.

This existing discrepancy between the availability of models and studies focusing on seismic energy radiation from rivers as well as debris flows (see, e.g., Burtin et al., 2008; Gimbert et al., 2014; Kean et al., 2015; Lai et al., 2018; Tsai et al., 2012), compared to infrasound (Schmandt et al., 2013), partly explains why the mechanism of infrasound radiation by debris flow has not been really investigated yet in depth. Most of the studies available (Hubl et al., 2013; Kogelnig et al., 2014; Li et al., 2012) up to now mostly focused on event detectability for monitoring purposes.

The wide range of monitoring and detection approaches (see Arattano & Marchi, 2005, for a review) reflects the technical challenges inherent to debris flow early warning. On one hand, debris flows typically move at moderate velocities of less than 10 m/s (Hurlimann et al., 2003), and thus early warning for downstream communities is possible if flows are detected quickly upon formation. On the other hand, high mountain torrents are difficult to access and subject to frequent rockfalls, landslides, and other mass movements. Consequently, instrumentation in lower catchment reaches is often preferable yet comes at the cost of reduced early warning time.

Among existing monitoring techniques, infrasound measurements have recently received particular attention, because in principle they do not require installations within or near a torrent. Instead, infrasound signals are detectable at distances up to hundreds of kilometers (see, e.g., Evers & Haak, 2001). The infrasound signal is generated as moving particles collide with atmosphere molecules and generate elastic air waves. Depending on flow rheology and attenuation in the air, the infrasound signal's frequency content of debris flows concentrates in a band below 40 Hz (Chou et al., 2013).

Though suited for remote detection, infrasound measurements of debris flows face key challenges: Infrasonic debris flow signals have emergent envelopes and lack impulsive, easily detectable phases. Moreover, torrent-related noise sources such as rockfalls, water flow, and above all wind can have amplitudes comparable to the debris flow signal (Bowman et al., 2005; Liu et al., 2015). Importantly, apart from a high noise floor, topographic barriers (e.g., mountain ridges and hills) between source and sensor also reduce the signal-to-noise ratio (Kogelnig et al., 2014; Lacanna & Ripepe, 2013; Lacanna et al., 2014).

In order to tackle these challenges, real-time trigger algorithms process debris flow signals in frequency space rather than time space to discriminate them from noise signals (Liu et al., 2015; Schimmel & Hübl, 2016). Detection reliability can be increased with concurrent recordings of ground motion using geophones colocated with the infrasound microphone (Hubl et al., 2013; Schimmel & Hübl, 2016).

Array techniques further improve detectability of infrasound sources. The technique enhances signal-to-noise ratios and distinguishes signal from noise in terms of source back azimuth and apparent infrasonic velocity. Array techniques are widespread in infrasound (see, e.g., Szuberla & Olson, 2004) and seismic (see, e.g., Rost & Thomas, 2002) monitoring. They have been used for the detection and monitoring of different kinds of gravity currents such as snow avalanches (Kogelnig et al., 2011; Marchetti et al., 2015; Ulivieri et al., 2011; Scott et al., 2007), pyroclastic flows (Barfucci & Ripepe, 2018; Ripepe et al., 2010), alpine

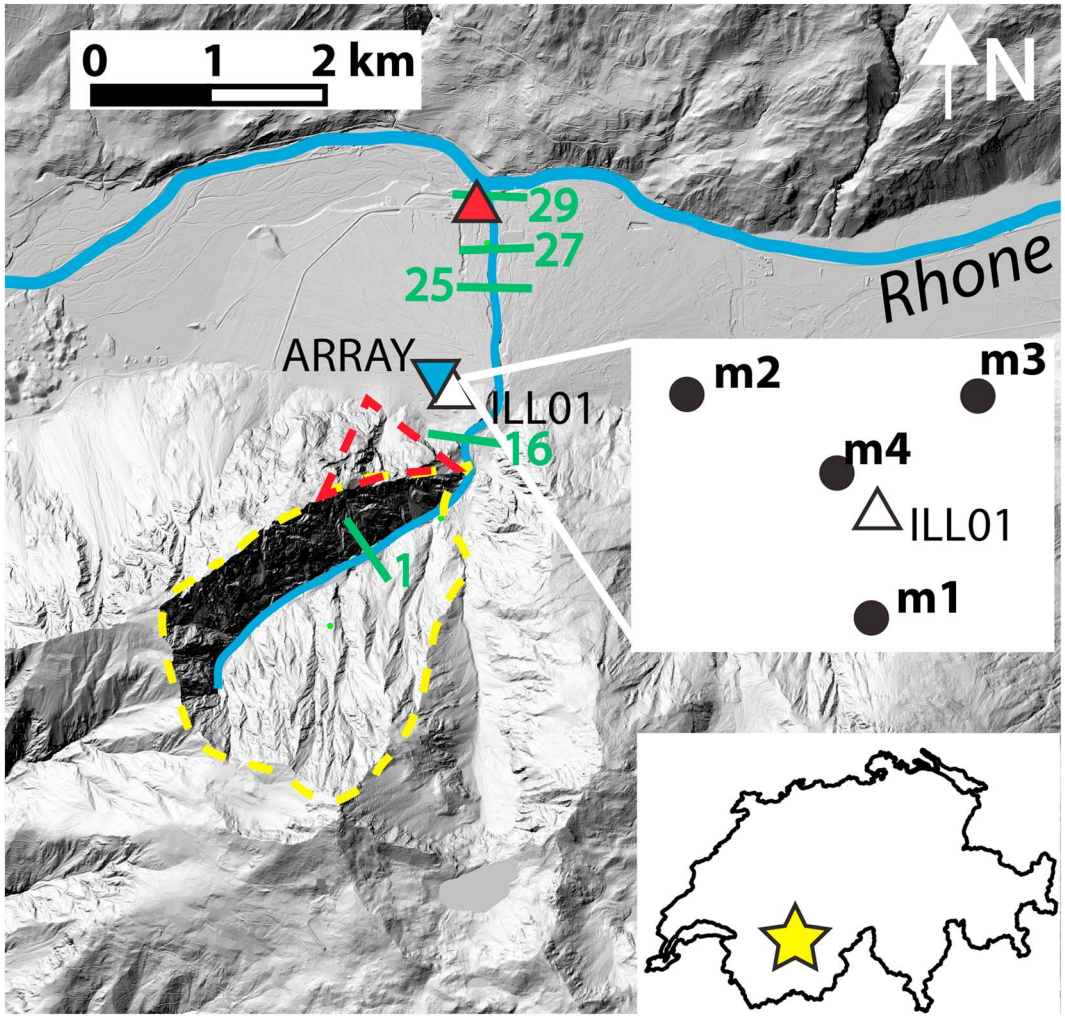

Figure 1. Illgraben catchment and Rhone valley in Switzerland's Canton Valais. Seismic sensor ILL01 is indicated by white triangle, infrasound array by blue upside-down triangle and automatic camera by a red triangle. Upper inset shows positions of four individual microphones (black-filled circles) making up the infrasound array. Lower inset shows Switzerland and location of Illgraben (star). Locations of selected CDs are presented by green bars with numerical labels. Dashed yellow line outlines an area that we refer to as upper catchment, while dashed red line marks the ridge between the array and CD1. CD = check dam.

glacier collapses (Preiswerk et al., 2016) and lahars (Johnson & Palma, 2015) but have yet to be applied to debris flows.

Here we use an infrasound antenna to study the infrasound radiation mechanism of debris flows at Illgraben, one of Switzerland's most debris flow-prone torrents. We combine seismic and infrasound observations to further investigate seismic-acoustic coupling and constrain the existence of multiple processes of elastic energy radiation in the ground and the atmosphere by the debris flow. Eventually, we investigate the efficiency of infrasound array monitoring to provide an early detection of the debris flow events with remote observations and investigate its potential as an early warning system compared to in situ observations.

2. Study Site

Illgraben is a steep torrent in southern Switzerland's Canton Valais and feeds directly into the Rhone River (Figure 1). It is about 5 km long draining a catchment area of 10 km^2. Debris flows with volumes of several tens of thousands of cubic meters occur on average 3–5 times per year and are a significant and sometimes dominant sediment supply mechanism from Illgraben to the Rhone River (Badoux et al., 2009; Rickenmann et al., 2001). The upper catchment has steep slopes of 40° or above producing frequent rockfalls or land-

Table 1
Parameter Estimations for the Three Largest 2017 Debris Flows at Illgraben Discussed in This Study

Date	Flow stage (m)	Velocity (m/s)	Volume (m^3)	Discharge (m^3/s)	CD 1 (UTC)	Infrasound (UTC)
29 May 2017	4.8	6.7	70,000	270	16:58:31	16:58:50
3 June 2017	3.3	4.3	24,000	150	23:27:38	23:27:28
14 June 2017	3.5	7.2	33,000	150	19:30:48	19:30:27

slides (Schlunegger et al., 2009). The largest landslide in recent decades occurred in 1961 and deposited 3,500,000 m^3 of material in the torrent. The main source of sediment generating debris flows at Illgraben is from the numerous landslides originating predominantly from steep slopes at the southern part of the catchment (Bennett et al., 2013). Debris flows typically occur in summer months when heavy precipitation mobilizes sediments in the channel or in steep gullies within lateral slopes (Berger et al., 2011). A series of check dams (CDs), most of which are situated on the inhabited debris fan in the Rhone valley (Figure 1) stabilizes the channel against erosion. As a result, most debris flows no longer overtop the channel bank and significant damage last occurred in 1961 when a road bridge was destroyed (Badoux et al., 2009).

The Swiss Federal Institute for Forest, Snow and Landscape Research WSL installed a scientific observatory (McArdell et al., 2007) and maintains an early warning system based on in-torrent debris flow detections (Badoux et al., 2009). The arrival times of the debris flow front are detected with geophones installed behind steel plates at CDs 1, 27, and 29 (Figure 1). The geophones provide voltage impulses induced by vertical vibrations as debris moves across their steel plates, and debris flow front arrival is defined when this signal exceeds a threshold voltage of 0.2 V. To calculate debris flow velocities near the Illgraben mouth, we use differences of the flow front's arrival time at CDs 27 and 29 (Figure 1). Furthermore, we measure flow stage

Figure 2. Picture of the front arrival of a debris flow at Illgrabenn (1 July 2008) taken from an automated camera (red triangle in Figure 1) operated by the WSL (Berger et al., 2011).

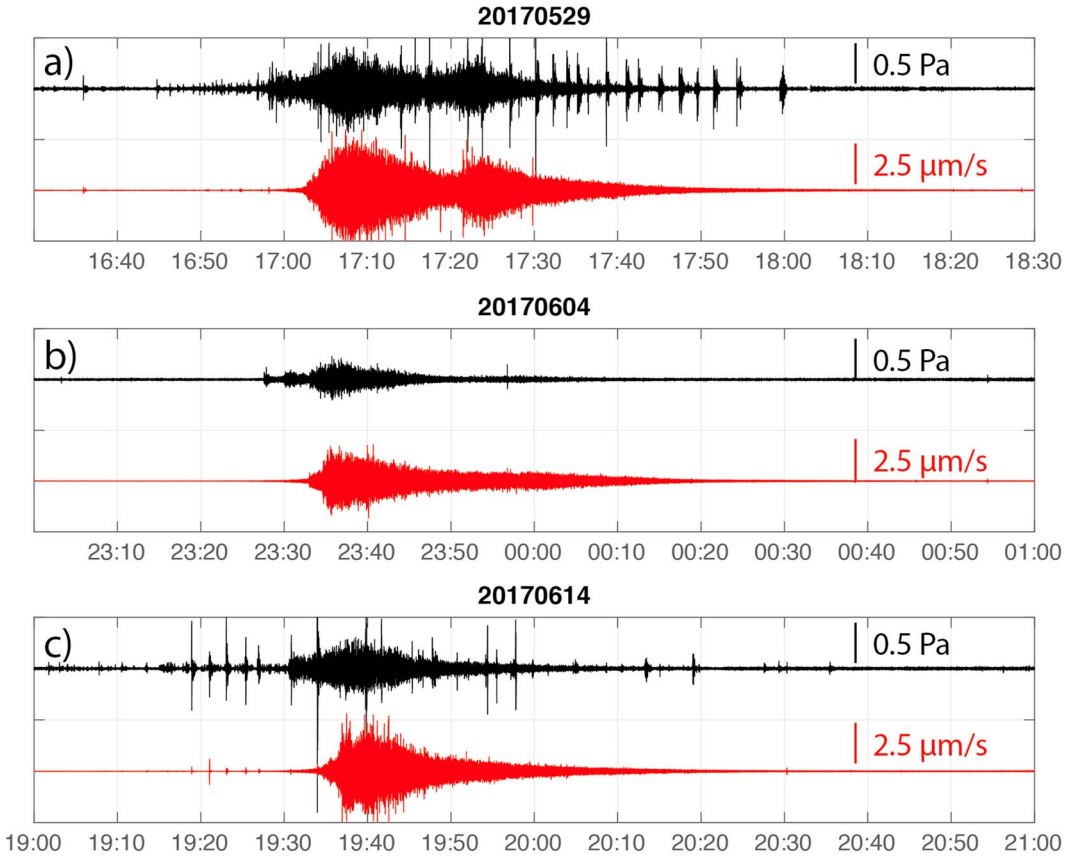

Figure 3. Infrasound (black) and seismic (red) records of debris flows recorded in 29 May (a), 4 June (b), and 14 June 2017 (c). Infrasound waveforms are band-pass filtered between 1 and 5 Hz.

using a laser altimeter suspended from a bridge across the channel at CD 29. From flow stage and flow velocity, we calculate discharge and total debris flow volume.

3. Instrumental Setup

The infrasound array was deployed north of the Illgraben in a flat forested area at an elevation of 750 m and at a distance of ≈0.6 km from Illgraben mouth (Figure 1). We used a FIBRA infrasound array (www.item-geophysics.it) that is designed to operate with fiber optic connection among up to five different array elements. Analogue pressure data are converted to digital at each array element at 50 Hz and 16 bits and are transmitted trough fiber optic to a central unit where data is synchronized, GPS time stamped, locally recorded, and made available trough the internet for data transmission. Power requirement is ≈1 W for the central unit and as low as ≈0.1 W for the array element. The use of an array with fiber optic allows to increase significantly the signal-to-noise ratio and prevents the risk of damages related to lightning or electric discharges. Each array element is equipped with a differential pressure transducer with a sensitivity of 400 mV/Pa in the pressure range of ± 12.5 Pa and frequency response between 0.01 and 200 Hz. For this study, we used four out of the five available channels and deployed the sensors with a triangular geometry in order to have the best azimuthal resolution. Array aperture (maximum distance between two array elements) is 160 m and is optimized to analyze infrasound signals in the frequency band between 1 and 10 Hz. The array was deployed on 15 May 2017 and operated continuously until 18 June 2017.

We installed a Lennartz LE3D 1s seismometer (ILL01 in Figure 1) recording all three dimensions of ground velocity with a flat response between the sensor's natural frequency of 1 and 80 Hz. The sensor was placed into a 30-cm-deep pit, which was subsequently filled up with sand. Ground motion was recorded with a Nanometrics Centaur digitizer at 100 Hz and continuously telemetered to the Swiss Seismological Service. The seismic sensor was colocated with the infrasound array north of the Illgraben in an easily accessible area.

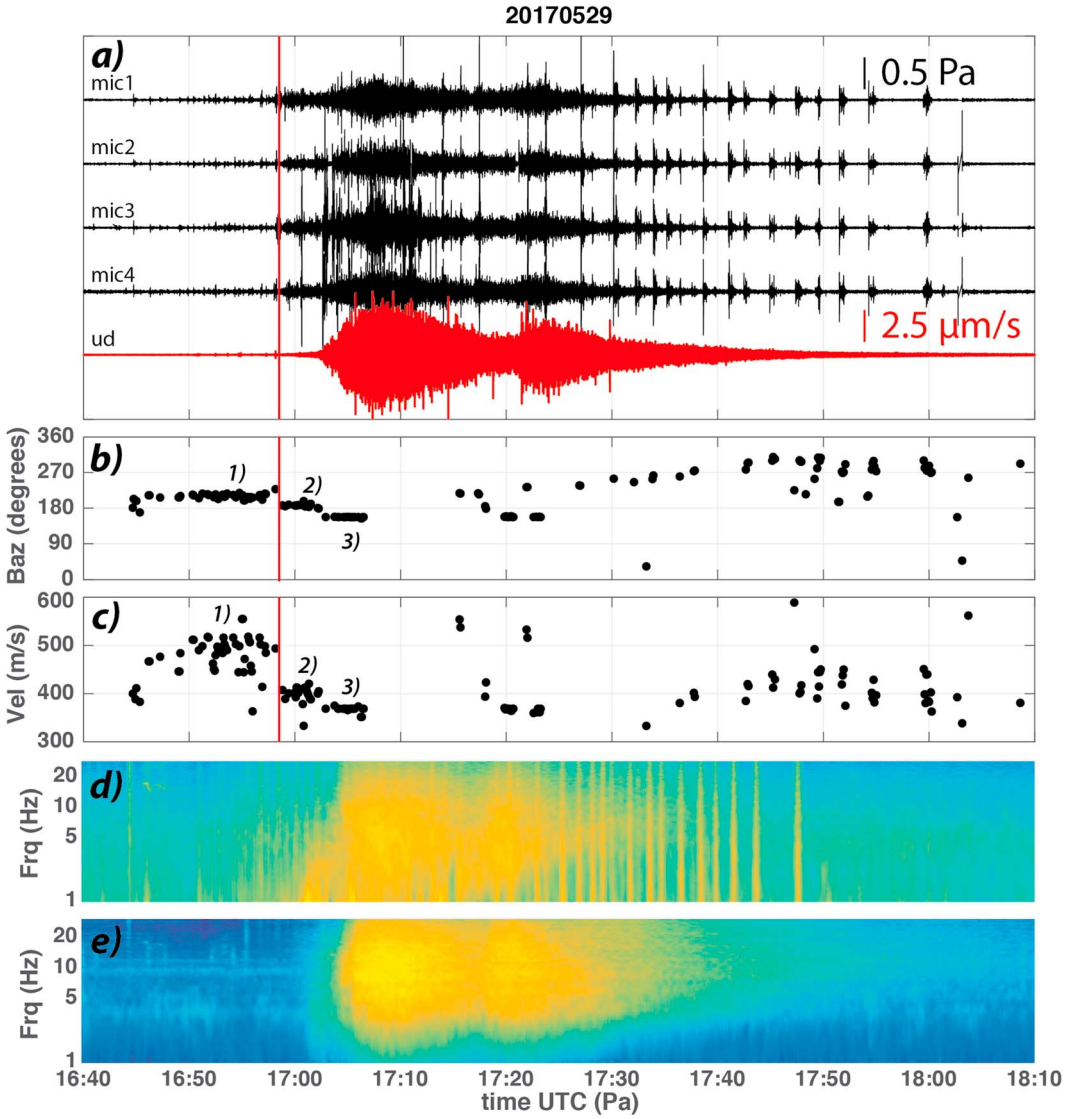

Figure 4. The 1.5-hr-long sample of infrasound array (black) and seismic (red) records of the 29 May 2017 debris flow event (a). Back azimuth (b) and apparent velocity (c) of infrasound detections. Normalized power spectral density (PSD) of infrasound (d) and seismic (e) records. The numbers in subplots b and c identify the different phases identified from infrasound array processing and discussed in the text. The red vertical line marks the arrival times at check dam 1 (Figure 1). Infrasound waveform in subplot a is band-pass filtered between 1 and 5 Hz.

For the present analysis, in addition to infrasound array and seismic data, we consider information on flow evolution provided by in-channel sensors installed at CDs 1 and 25 as well as the position of CD 16 (Figure 1 and Table 1). CD 1, built at an elevation of 1,090 m inside the Illgraben and with a height of ≈45 m, is positioned at a distance of 1,600 m from the array and has a corresponding back azimuth (direction from the dam to the array) of 200° N. The dam is not visible from the array being masked by the northern ridge of the Illgraben (dashed red line in Figure 1). Considering a straight line from the dam to the array along topography, the ridge reaches a maximum altitude of ≈1,200 m (450 m higher than the elevation of the array). CD 16 is on the contrary almost line of sight to the array (Figure 1), being positioned at an elevation of ≈850 m, a distance of ≈750 m from the array and with a back azimuth of 155° N. The distance between CDs 1 and 16 along the channel of the Illgraben is ≈1,400 m with an elevation difference of ≈200 m (mean slope of 15%) from the base of the CD 1. CD 25 is positioned at an elevation of ≈700 m and a distance of ≈900 m from the array. The corresponding back azimuth is 35° N. The along-channel distance between CDs 16 and 25 is ≈1,500, and the minimum distance between the Illgraben channel and the array of ≈500 m is

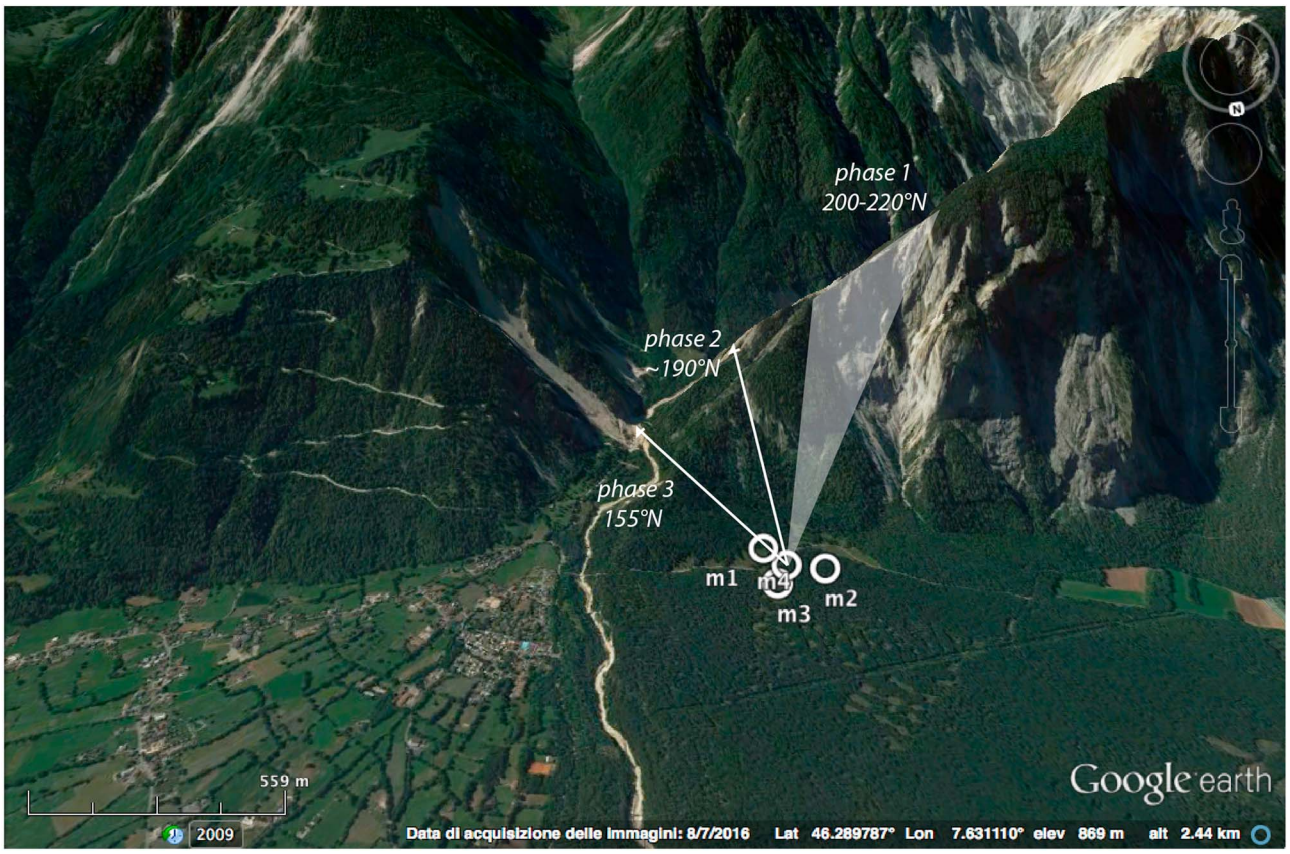

Figure 5. Google Earth projection of back azimuth of the three phases identified from infrasound back azimuth during the initiation of the 29 May 2017 event and highlighted in Figure 1.

approximately half the way between CDs 16 and 25 (Figure 1). CDs 1 and 25 are equipped with geophones providing the exact timing of the debris flow passage.

4. Debris Flow Events

Our study focuses on three debris flows (Figure 2), which occurred in 2017 (Table 1). All three events were large compared to typical debris flows at Illgraben (Badoux et al., 2009) and the largest one (29 May 2017) had a volume of 70,000 m^3, which is close to the mean annual supply of sediment (100,000 m^3) from Illgraben to the Rhone River (Schlunegger et al., 2009). The event on 14 June 2017 was furthermore exceptionally large moving at a velocity of 7.2 m/s between CDs 27 and 29.

All events are recorded as emergent seismic and infrasonic signals of long duration (30–40 min), with peak infrasonic amplitude for the long-lasting emergent phase of 0.5 Pa and peak seismic amplitude of ≈2.5 μm/s (Figure 3). The May 29 event, in particular consists into two main flows, one after the other, with the second event slightly shorter (≈10 minutes) and of smaller seismic (1.5 μm/s) and infrasonic (0.3 Pa) amplitude than the first event. From Figure 3 it is evident how the 4 June and 14 June debris flows differ from the 29 May event for the presence of a faster increase of the seismic signal, while the rise phase of the 29 May event is more gentle.

The 29 May and 14 June events are also characterized by high-frequency transients that overimpose on the spindle-shaped signals produced by the debris flow that are much clearer and of larger amplitude (≥1 Pa) in the infrasound record rather than in the seismic. These transients are produced by lightning and subsequent infrasound radiated by the thunder and propagating across the array (see Appendix A).

4.1. Infrasound Array Analysis of Debris Flows

An infrasound array consists on multiple infrasonic sensors deployed in the field and used as an antenna. It allows reducing the signal-to-noise ratio and identifying signal, which, unlike noise, is coherent across the

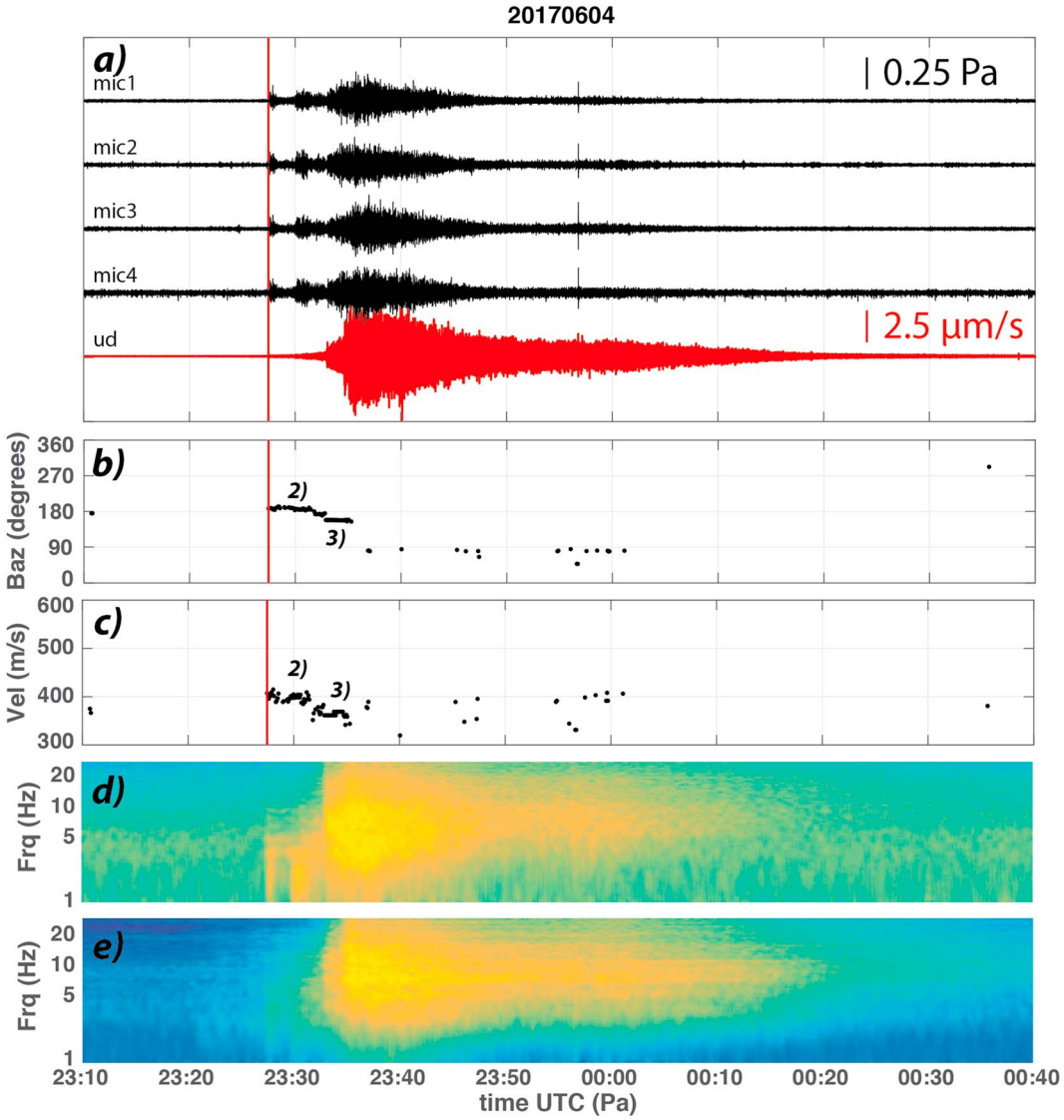

Figure 6. The 1.5-hr-long sample of infrasound array (black) and seismic (red) records of the 4 June 2017 debris flow event (a). Back azimuth (b) and apparent velocity (c) of infrasound detections. Normalized PSD of infrasound (d) and seismic (e) records. The numbers in subplots b and c identify the different phases identified from infrasound array processing and discussed in the text. The red vertical line marks the arrival times at check dam 1 (Figure 1). Infrasound waveform in subplot a is band-pass filtered between 1 and 5 Hz.

elements of the array, in terms of back azimuth (B_{az}) and apparent velocity (C_a). While the former identifies the direction of infrasound wave propagation, the latter corresponds to the velocity the wave would have if it was propagating in plane fitting the array and is defined as the real propagation velocity (c) divided by the sine of the take off angle ($C_a = c/\sin\gamma$).

The analysis of infrasound array data was performed by calculating the correlation between data recorded at the different elements of the array. For this study, the analysis is applied over 10 s-long time windows with 5 s of overlap on infrasound data band-pass filtered between 1 and 10 Hz. For each time window of analysis, a detection is identified whenever coherent data are recorded across the array, and time delay among array elements is used to calculate back azimuth and apparent velocity of the infrasonic wavefield. Details about the infrasound array processing are provided in the Appendix B.

Array processing of infrasound records of the 29 May 2017 event (Figure 4a) shows that coherent infrasound signal is recorded only during the initial part of the flow and highlights the existence of three phases characterized by stable values of back azimuth and apparent velocity (Figures 4b and 4c). The first phase (1 in

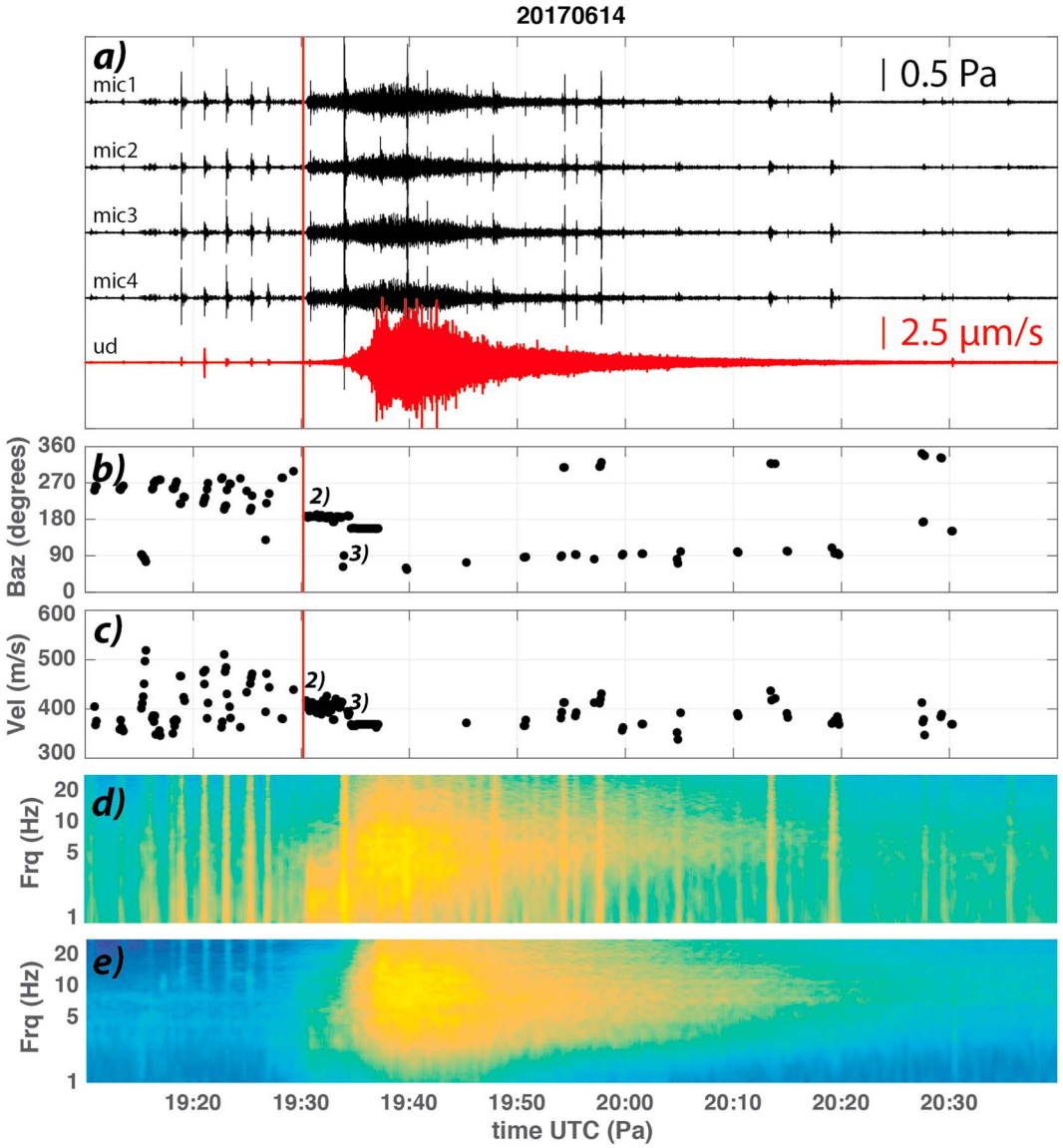

Figure 7. The 1.5-hr-long sample of infrasound array (black) and seismic (red) records of the 14 June 2017 debris flow event (a). Back azimuth (b) and apparent velocity (c) of infrasound detections. Normalized PSD of infrasound (d) and seismic (e) records. The numbers in subplots b and c identify the different phases identified from infrasound array processing and discussed in the text. The red vertical line marks the arrival times at check dam 1 (Figure 1). Infrasound waveform in subplot a is band-pass filtered between 1 and 5 Hz.

Figure 4b) starts around 16:45 UTC, ≈15 min before the debris flow is observed at the CD 1 (16:58:31 UTC). The signal is recorded with a back azimuth of 200–220° N and high values of apparent velocity (480 m/s) that suggests pressure waves produced inside the Illgraben and propagating across the ridge (dashed red line in Figure 1) to be eventually recorded at the array (Figure 5). Considering a propagation velocity of sound (c) around 340 m/s, the measured apparent velocity of 480 m/s is consistent with a takeoff angle (θ) of 45°. This value is in quite a good agreement with a pressure wave produced inside the Illgraben and crossing the ridge that is approximately 800 m far and 600 m higher than the array (Figure 5).

This first phase lasts approximately 15 min until 17:00 UTC, when the second phase (2 in Figure 4b and 4c) starts being characterized by lower values of back azimuth (≈190° N) as well as apparent velocity (≈400 m/s; Figure 4b and 4c). This direction of propagation matches with CD 1, positioned within the Illgraben at a distance of ≈1,600 m from the array. Infrasound produced at the dam crosses the mountain ridge (dashed red line in Figure 1) to be eventually recorded at the array, after a propagation time of ≈5 s. The lower value of

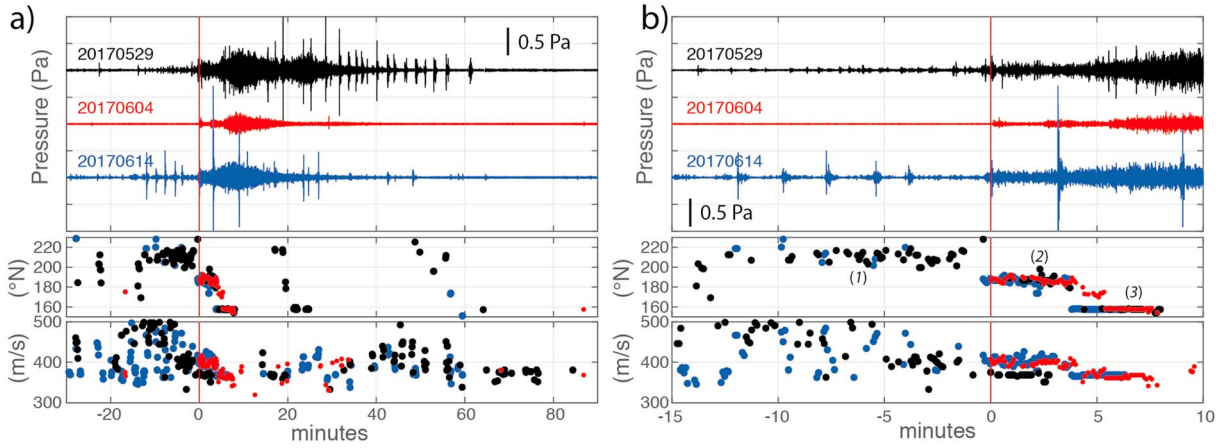

Figure 8. The 90-min-long example (a) and 25-min-long detail (b) of pressure records, back azimuth, and apparent velocity for the three debris flow events aligned according to the time of detection at check dam 1 (red vertical line).

measured apparent velocity form phase 1 is consistent with the lower elevation of the ridge along the ≈190° N back azimuth direction from the array. While the debris flow is flowing downhill along the Illgraben, infrasound continues to be recorded persistently from ≈190° N, the 45-m waterfall at CD 1 being the most energetic source of sound. This is in agreement with experimental and theoretical studies of infrasound produced at waterfalls and dams (Feng et al., 2014; Kudo, 1993).

Eventually when the flow exits the valley and reaches CD 16 (Figure 1) infrasound starts abruptly to be recorded with a different back azimuth (155° N) pointing directly to the dam (phase 3 in Figures 4b and 4c). For the specific case of the 29 May event, infrasound signal from this same back azimuth is recorded also between 17:19 and 17:23 UTC, when a second flow reaches the dam. Similarly to what was inferred for phase 2, we suggest that the increased infrasound radiation produced by the waterfall (Feng et al., 2014; Kudo, 1993) at the dam is the most energetic source of infrasound that is detected as a stable source although the flow keeps moving downhill.

This peculiar variation of back azimuth and apparent velocity is observed for all recorded events (Figures 6–8), suggesting that a stable mechanism of infrasound radiation during the debris flow evolution at Illgraben exists. In particular all events are characterized by infrasound radiation from stable sources during the initial phase of the event (phases 2 and 3), while no more detections of infrasound signal are observed despite the infrasound amplitude keeps increasing.

The precursory infrasound of phase 1 is observed only for the 29 May event. Based on wave parameters (back azimuth and apparent velocity), we suggest that this phase possibly reflects debris flow initiation within the graben, able to radiate infrasound that is crossing the mountain ridge (dashed red line in Figure 1) and is recorded at the array (Figures 4b and 4c). However, we cannot exclude that such signals might be radiated by small landslides occurring on the northern flack of the ridge, as the back azimuth (200–220° N, Figure 5) is indeed pointing to a sector of the ridge that is strongly eroded. Future observation will be required to further investigate this aspect.

4.2. Spectral Analysis of Debris Flows

Spectral analysis of seismic and infrasound records (subplots d and f of Figures 4, 6, and 7) shows how the seismic signal of the debris flow is characterized by a broad spectrum from few hertz up to >25 Hz and peaked around 8 Hz, without any obvious systematic variation in the spectral content through time. On the contrary, the infrasound spectrum shows a low-frequency component (<2 Hz) at the beginning of the event, which increases through time, before a broad frequency content (between 2 and 10 Hz and peaked around 5 Hz) is recorded abruptly (Figure 4, 6, and 7).

The comparison with the timing of infrasound detections helps clarifying the recorded spectrogram. The abrupt increase of the infrasound frequency content observed for all events corresponds indeed to the time of the first detection with back azimuth of 155° N that marks the arrival of the debris flow at CD 16 at the Illgraben mouth. The low-frequency infrasound recorded before is thus produced by the flow, while it

is still flowing within the Illgraben and is recorded at the array after crossing the ridge (dashed red line in Figure 1), while signal recorded afterward has line-of-sight propagation to the array. Consistently with modeling and observation of topography effects on short-range infrasound records (Lacanna et al., 2014; Lacanna & Ripepe, 2013), the ridge does not prevent infrasound being recorded but strongly attenuates the high-frequency component of the signal, while lower-frequency component is much less affected.

5. Discussion

Results derived from array analysis of infrasound data and comparison of the spectral content of infrasound and seismic data, as presented in the previous section, suggest a complex mechanism of infrasound and seismic energy radiation by the debris flow. In this section, we first investigate the mechanism of infrasound radiation, discuss the coupling of the seismic and infrasound sources and eventually discuss the possible use of infrasound array analysis as a remote early warning system for debris flows.

5.1. Mechanisms of Infrasound Radiation by Debris Flow at Illgraben

The infrasound array analysis, combined with the timing provided by the instrumented CDs can be used to provide insights on the dynamics of the flow. Figure 8 shows the detail of the infrasound detections for all events, aligned according to the detection time at CD 1 provided by the geophone. The figure clearly shows that all events share phases 2 and 3, while phase 1 is recorded only during the major event of 29 May 2017.

Stable detections characterizing phase 2 start exactly when the debris flow passes CD 1 for all events (Figure 8b) and continues for a time period of 3–4 min even though the flow is moving downhill, until phase 3 starts. This is marked by an abrupt change in the back azimuth and apparent velocity of infrasound detections and corresponds to the time the debris flow reaches CD 16 (Figure 1). By that time, it starts radiating infrasound from this fixed position that remains stable for several minutes even though the flow keeps moving downhill. This is consistent with theoretical and experimental studies of infrasound radiated at waterfalls and dams (Feng et al., 2014; Kudo, 1993).

Detecting a stable source position in case of moving sources is not unexpected and is a consequence of infrasound array analysis that, in case of multiple sources, detects preferentially the most energetic one. Such a behavior has been observed already for snow avalanches (Marchetti et al., 2015) and pyroclastic density currents (Delle Donne et al., 2014) passing a discontinuity in the topography where infrasound energy radiation focuses in a stable position. However, snow avalanches and pyroclastic density currents produce a coherent infrasonic signal all along their downhill moving front and array analysis allows to clearly track their movement (Delle Donne et al., 2014; Marchetti et al., 2015).

For the debris flow events, we observe that coherent infrasound is recorded only when the flow crosses the dams (Figure 8), while it is not detected by the array otherwise although the signal amplitude is high and the frequency content is relatively low (<10 Hz). This indicates a lack of coherence. Figure 9 shows the normalized envelope of the infrasonic (black) and seismic (red) signal compared to the timing of the flow at the different check dams (CDs 1, 16, and 25; red lines) and the end time of phase 3 (blue line), that marks the end of coherent infrasound.

For all cases, infrasound starts increasing 10–20 min before the colocated seismic signal (Figure 9). A significant departure between the infrasonic and seismic envelope is observed already before the flow reaches CD 1, suggesting that infrasound radiated by the flow is able to cross the mountain ridge (dashed red line in Figure 1) to be recorded at the array while no clear seismic signal is recorded at ILL01 station. After the flow reaches the CD 16 and enters the Rhone valley, also the amplitude of the seismic signal recorded at ILL01 station starts increasing. This is consistent with previous observations performed by Hubl et al. (2013) and Kogelnig et al. (2014) who recorded infrasound and seismic signals after the flow entered the Rhone valley and suggested that earlier infrasound detections were possibly masked by topography effects.

When phase 3 ends (blue line in Figure 9), coherent infrasound at the array is no more detected (Figure 8) but the envelopes of seismic and infrasound signals keep rising through time clearly indicating that more and more elastic energy is radiated by the flow in the air and in the ground. However, maximum amplitude is not recorded when the flow head reaches the minimum distance of the channel to the array (≈500 m), approximately half the way between CDs 16 and 25, as would be expected in case of a simple moving point source. For all cases, when maximum amplitude is recorded, the flow has already reached CD 25, ≈700 m

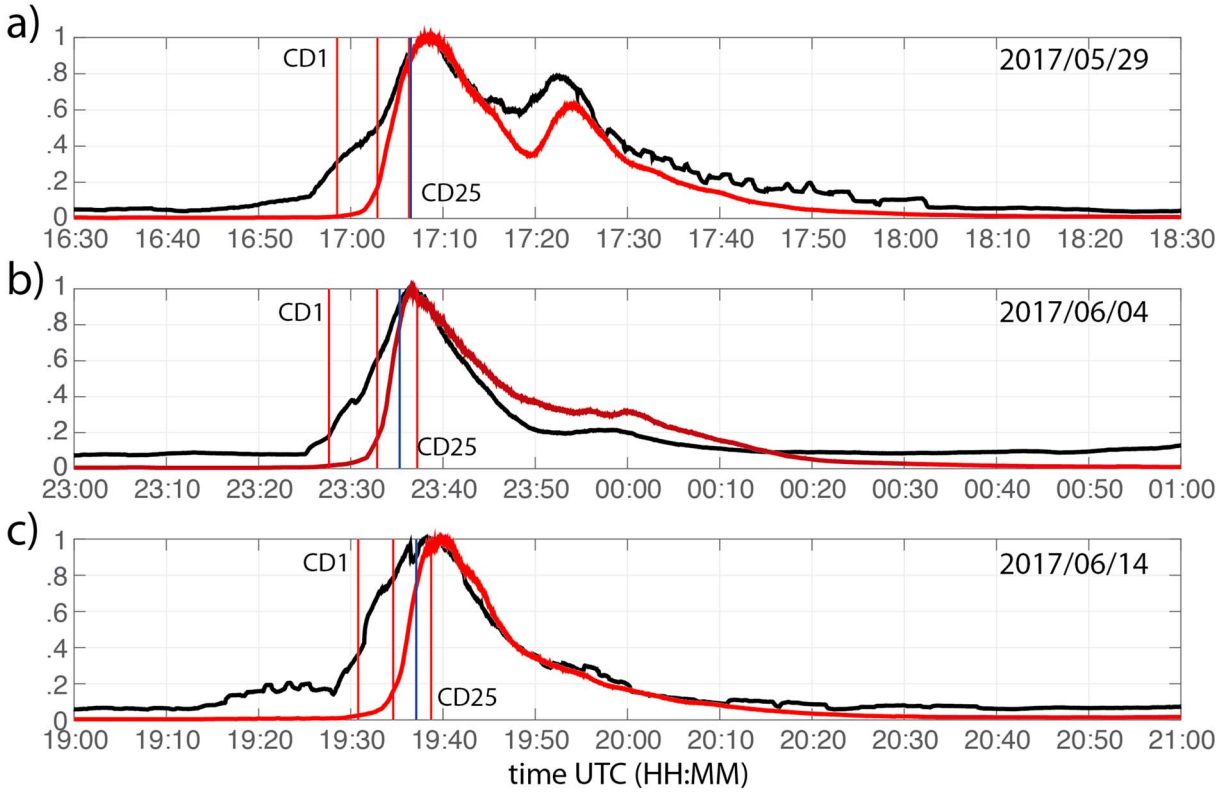

Figure 9. Normalized envelope of infrasound (black) and seismic (red) signals recorded by the three debris flows. Red vertical lines mark the timing of the debris flow at CDs 1, 16, and 25, with the timing at CD 16 inferred from infrasound array analysis and timing at CDs 1 and 25 measured directly at the dam with geophones. The blue vertical line marks the end time of phase 3 (Figure 8) of infrasound detections. CD = check dam.

more distant than the minimum distance to the array. Only afterward infrasound and seismic amplitude decrease following a similar trend.

5.1.1. Numerical Simulation of Infrasound Radiated by an Extended Source

The infrasound array analysis presented above points to a complex mechanism of infrasound radiation by the debris flow at Illgraben. Infrasound is indeed radiated at the dams that appear as stable sources of energy, even though the flow keeps moving downhill. Yet the main part of the signal, despite being characterized by high amplitude and low frequency, shows low coherence and is thus not detected by the array processing.

In order to investigate the lack of coherent infrasound and thus not detectable by array processing, we modeled the infrasound radiated by an extended linear source and investigated the array detectability. Infrasound from rivers is indeed believed to be produced by free waves at the water surface (e.g., Schmandt et al., 2013). Therefore, multiple sources will be active simultaneously and at different locations, when water is flowing in a river.

Figure 10 shows a sketch of the problem. We consider a linear source of length (L) of 500 m, formed by 50 different point sources of infrasound, positioned 10 m apart from each other, and moving with a horizontal velocity (u) of 10 m/s. A spacing of 10 m between adjacent sources is consistent with observation of the free waves at the surface of debris flow. The head of the linear source of infrasound (black in Figure 10a) reaches the minimum distance to the array, that corresponds to 300 m from mic2 in Figure 10, at time $t = 50$ s and with corresponding back azimuth to the array of 270° N.

Each source is assumed to produce a pressure wave in the atmosphere with an amplitude of 1 Pa and a peak frequency of 3 Hz, in accordance with observed spectra of infrasound radiated by debris flows at Illgraben (Figures 4, 6, and 7). Random noise is added to the infrasound waveform radiated by each point source, and a random phase shift is allowed for the extended source. This assures that at the same given time, the different point sources of the extended source can radiate infrasound with the same amplitude and same frequency but with a different phase. The resulting infrasonic waveform at each element of the array is

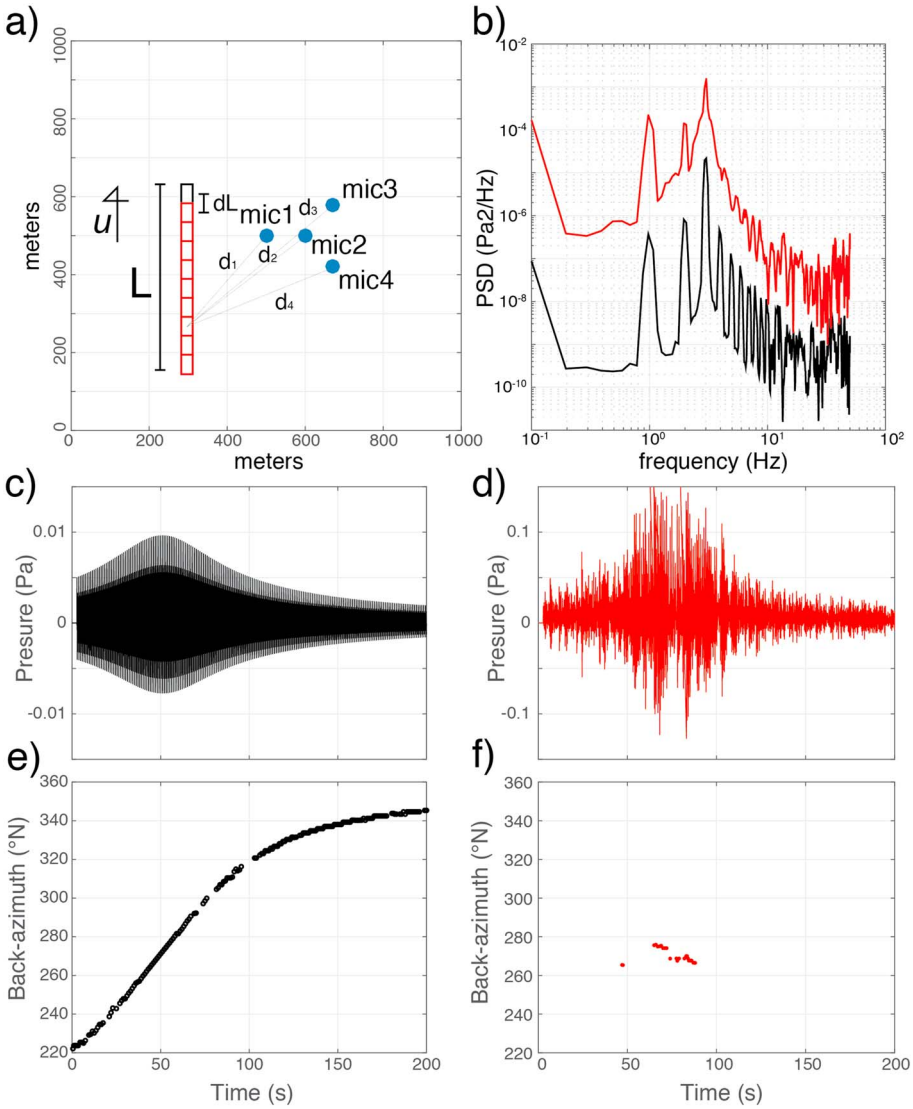

Figure 10. (a) Sketch of an extended moving source simulating a flow and radiating infrasound recorded by an infrasound array. We assume elastic energy being radiated only at the head of the flow (black) or by the whole flow (black and red). Infrasound signals and detections at the array in case of elastic energy being radiated by the point source (c, e) or by the extended source (d, f), and corresponding power spectral density (b).

obtained considering the whole contribution for all sources through time, corrected for both propagation time and attenuation.

We first consider infrasound being produced only a single point source at the head of the flow (black in Figure 10a). The simulated infrasound signal recorded at mic1 of the array has a cigar-shape envelope with the maximum amplitude recorded after 50 s (Figure 10c). The signal is highly coherent and infrasound array processing allows to easily track the movement of the source in terms of back azimuth variation through time (Figure 10e).

The simulated infrasound signal recorded at mic1 considering the contribution of 50 point sources has a cigar-shape envelope, similar to the point source, but its maximum amplitude is recorded after 75 s (Figure 10d). The delay of 25 s is required for the barycenter of the extended source to reach the minimum distance to the array (i.e., 250 m at 10 m/s). Moreover, the contribution of multiple sources, despite maintaining the amplitude, waveform characteristics (Figures 10c and 10d) and spectral content (Figure 10b) similar to a moving point source, results in a dramatic decrease of signal coherence that prevents the possibility to track the source with array processing (Figure 10f).

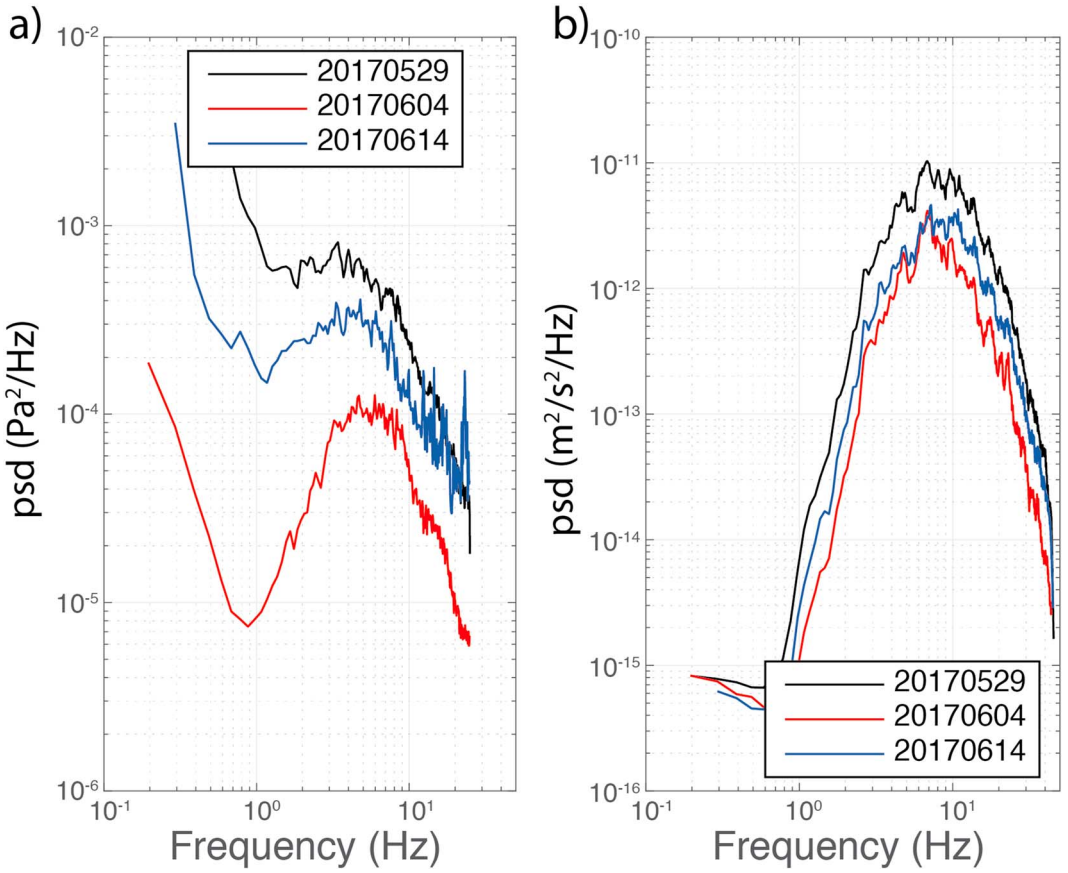

Figure 11. Power spectral density of infrasound (a) and seismic (b) records of the three debris flow events.

This simple example allows consolidating a model of infrasound radiation by debris flow, with free waves at the water surface along the entire flow length radiating elastic energy to the atmosphere, with variable phase. These contribute to a spindle-shape signal of amplitude exceeding 0.5 Pa at a distance of >500 m from the source but with low coherence. Therefore, array processing is not really useful to track and investigate the flow, unless discontinuity points of the topography, such as change of slopes or dams, result in stable sources of infrasound clearly detectable by the array. We suggest therefore that the mechanism of infrasound radiation by debris flow is different from other density currents like snow avalanches or pyroclastic density currents, where a turbulent head develops radiating elastic energy in the atmosphere, that allows to nicely track the flow evolution through time with an infrasound array (e.g., Delle Donne et al., 2014; Marchetti et al., 2015; Ulivieri et al., 2011).

5.2. Seismoacoustic Coupling of Radiated Elastic Energy

Figure 11 shows the mean power spectral density of seismic and infrasound signals for the three debris flow events. This was calculated considering the entire waveforms of Figure 3 and by applying spectral analysis over 10-s-long windows with a superposition of 50 %. The PSD of the seismic signals (Figure 11b) is very stable for all events, peaking around 8 Hz, with a spectral amplitude that scales with the recorded discharge rate. The spectrum drops quickly both for low (<3 Hz) and high (>20 Hz) frequencies. Based on the model proposed by Tsai et al. (2012), for seismic noise produced by bed load transport, the frequency content of the seismic spectrum is mostly dominated by the source-to-receiver distance. The observed peak around 8 Hz is in good agreement with the minimum distance of ≈500 m to the Illgraben torrent.

Similarly to what observed for seismic signal, the PSD of recorded infrasound is very stable for the three debris flow events, with a constant frequency content (peaking around 5 Hz) regardless the flow discharge but showing a spectral amplitude that appears to scale with the volume of the flows (Figure 11a). In agreement with the modeling of infrasound wave radiation presented above and with what suggested by Schmandt et al. (2013) for a controlled flow experiment at Grand Canyon, we suggest that the fluid-air inter-

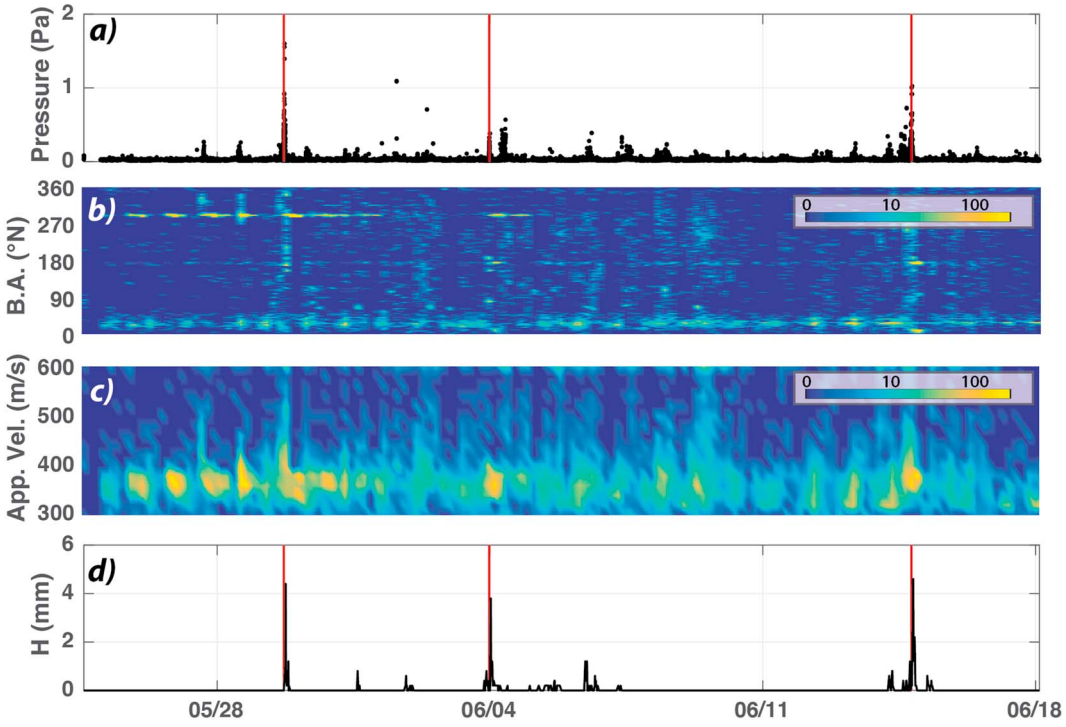

Figure 12. Results from infrasound array processing between 24 May and 18 June 2017, showing excess pressure (a), back azimuth (b), and apparent velocity (c) of infrasound detections. Color bars indicate the number of detections every 4 hr. (d) Cumulative precipitation (mm) over a time period of 10 min. Vertical red lines identify the timing of automatic detection of the debris flow event based on infrasound array analysis (Table 1).

action such as breaking waves is the most likely source mechanism of elastic energy around 5 Hz. However, unlike what was reported by Schmandt et al. (2013), who observed a spectral coupling between seismic and infrasound records, in our case, the seismic and infrasound signals seem to be decoupled.

Such a discrepancy might depend on the different source-to-received distances for the two experiments. In our case, infrasound and seismic data were indeed recorded at a much larger distance from the channel (≈500 m) than for the Grand Canyon experiment (≈35 m). At such distances, seismic energy produced by fluid-air interaction might indeed undergo a larger attenuation than infrasound. This might explain the lack of the spectral coupling between the two signals, with seismic data only affected by the spectral peak induced by bed load transport.

5.3. Use of Infrasound Monitoring as an Early Warning System for Debris Flows

Array analysis of continuous infrasound data recorded between 24 May and 18 June 2017 allows identifying the general infrasound activity around the array (Figure 12). During this 1-month-long period, the array processing identified >20,000 detections, resulting in coherent infrasound recorded approximately 10% of the time. This includes the three debris flow events as well as additional signals produced by natural and anthropogenic sources of variable strength and duration.

Infrasound excess pressure at the array is generally of low amplitude (<2 Pa), with maximum amplitude recorded during the 29 May debris flow event (Figure 12a). Infrasound detections are typically characterized by low values of apparent velocity (<400 m/s) and highlight several persistent sources around the array. Figure 12b shows coherent, sustained infrasound with back azimuth of ≈25 (±15), 174 (±3), and 292 (±2)° N, suggesting the existence of repetitive sources through time. The first cluster of infrasound detections ($B_{az} \approx 25 \pm 15°$ N) is likely related to signal produced within the town of Leuk, located northeast of the array at a distance of ≈2 km. Concerning the detections with back azimuth centered around 174° N, we suggest they might be consistent with the activity within Illgraben, as it is pointing toward the mouth of Illgraben torrent entering the Rohne valley. The last cluster of detections characterized by a back azimuth value centered at 292° N (Figure 12b) is pointing directly to the dam of the Tseuzier lake, positioned at a distance of 15 km from the array.

Going into the details of the sources driving the different clusters of infrasound detections is beyond the scope of the present work, but a general description of the sensitivity of the infrasound array is required to tune a possible procedure for automatic detection of debris flow events. From Figure 8 it is evident that all the debris flow events share a phase of stable detections from the back azimuth of 155° N that corresponds to CD 16 right at the mouth of the Illgraben (phase 3 in Figure 8b). This is preceded by a phase of infrasound detections with a back azimuth of ≈180–190° N, and an apparent velocity (≈400 m/s) that we showed reflects the flow at CD 1 (phase 2 in Figure 8b).

In order to identify automatically the infrasound signal produced by the debris flow, we propose to use the observed peculiar trends of infrasound detections recorded for all the three events (Figure 8b). We suggest indeed that it is a clear signature of debris flow occurrence at Illgraben and is not to be expected from different sources of infrasound acting at various distances around the array. In detail, we follow the procedure described by Ulivieri et al. (2011) and on the basis of time persistency of detections that are directly calculated with the infrasound array processing discussed in Appendix B, we group detections into signals (i.e., group of detections close in time with stable characteristics of back azimuth and apparent velocity). Afterward, we scan all infrasound data recorded between 24 May to 18 June 2017 and extract only those signals whose back azimuth and apparent velocity are consistent with phase 2 and phase 3 of infrasound from debris flows at Illgraben (Figure 8b). Eventually, only the three debris flow events have been identified without any false alerts during the period of investigation (Figure 12). The onset time of the automatically detected infrasound signals (Table 1) is comparable to timing of the debris flow obtained from the sensors installed at CD 1, inside the Illgraben. This result, which might be obtained in near real time with infrasound array processing, is showing that infrasound can be used to monitor and detect efficiently the occurrence of debris flow events at Illgraben torrent. By using the proposed infrasound array processing and detection algorithm at Illgraben, it might indeed be possible to detect the occurrence of an event from a remote location, with a timing that is in quite a good agreement with the timing provided by instrumented CD 1 inside the canyon, whose installation, operation, and maintenance poses considerable technical challenges.

6. Conclusions

In this work, we present a seismoacoustic analysis of debris flow activity at Illgraben torrent, Canton Valais, Switzerland, focusing on three debris flow events that occurred in spring 2017 with total volume spanning from 24,000 to 70,000 m^3. Infrasound data were collected with a small aperture array, deployed in a forested area on the Illgraben fan in the Rhone valley, easily accessible for deployment and maintenance. Debris flows are recorded as emergent signals of long duration both in the seismic and infrasound record.

Infrasound and seismic data show a stable frequency content peaking around 8 Hz for the seismic and between 3–5 Hz for the infrasound. In both cases, spectral amplitude scales with the flow discharge, with maximum amplitude recorded during the 29 May 2017 debris flow event. Based on the observed frequency content, we suggest that seismic and infrasound likely reflect two separate processes. Seismic is mostly affected by bed load sediment transport, with a constant peak frequency of ≈8 Hz mostly controlled by the minimum distance between the flow and recorder of 500 m. Infrasound is most likely produced by waves at the river free surface. Unlike what was observed for a controlled flood experiment at Grand Canyon (Schmandt et al., 2013), we do not observe any significant coupling between seismic and infrasound data.

Infrasound array analysis showed that clear infrasound signal from Illgraben is detected shortly after the flow initiation phase, with infrasound wave parameters indicating a stable source that coincides with the first check dam (CD 1), installed within the Illgraben valley at a distance of ≈1,600 m from the array. Despite not being line of sight to the array, the infrasound signal is able to cross the mountain ridge (dashed red line in Figure 1) to be recorded at the array, with the effect of topography resulting in a low-pass filter (Figures 4, 6, and 7d). A second phase of infrasound detections is recorded when the flow enters the Rhone valley. Again, the stable wave parameters (back azimuth and apparent velocity) point to a fixed source corresponding to the first check dam immediately outside the Illgraben (CD 16). Eventually, no more infrasound detections are recorded despite raising infrasound amplitude.

Based on the stable detections from fixed sources and the lack of detections during the peak amplitude phase of infrasound envelope, we present a model of infrasound radiation by debris flow, in terms of an extended source, that consists into muliple point sources, moving with constant velocity. A synthetic pressure wave is constructed assuming an extension of the flow of 500 m, moving at 10 m/s and radiating 3-Hz pressure wave

with random phase from 50 discrete point sources along its length. Consistent with real data, the resulting signal has a spindle-shape envelope, of long duration, whose maximum amplitude is recorded when the barycenter of the extended moving source reaches the minimum distance to the array. The variable phase of infrasound radiated by the multiple-point sources, despite maintaining the frequency content of recorded signal and contributing to the amplitude, lacks coherence thus preventing infrasound array detections. Such a model appears consistent with the free waves at the water surface, typically showing random phase at the scale of the flow.

The proposed mechanism of infrasound radiation by debris flow is different from other density currents like snow avalanches of pyroclastic density currents. Here a turbulent head develops along the flow radiating elastic energy in the atmosphere that allows tracking the flow evolution through time with an infrasound array (e.g., Delle Donne et al., 2014; Marchetti et al., 2015; Ulivieri et al., 2011).

Although the characteristics of the source prevents array detections, we showed that discontinuity points of the topography, such as change of slopes or dams, result in stable sources of infrasound clearly detectable by the array. For the specific case of Illgraben torrent, the infrasound array proved to be able to efficiently detect infrasound produced at CD 1 (Figure 1), without any false alarms. Using the persistent characteristics of recorded wave parameters, we showed how the infrasound array could be used to identify remotely, from an accessible location, the occurrence of the flow as early as at CD 1, thus representing a valuable system for automatic alarm for debris flow events. For the 29 May event, an even longer precursory phase is clearly identified (phase 1, Figure 4), that might extend even more the prealert for the flow. The corresponding infrasound wave parameters (back azimuth and apparent velocity) suggest that it might possibly be produced by the initiation phase of the flow before it reaches CD 1, but additional data will be required to further analyze this aspect.

Appendix A: Lightning Activity

The 29 May and the 14 June debris flow events are punctuated by discrete transients of large amplitude (up to 1 Pa) and short duration (<30 s), recorded clearly in the infrasonic and seismic data and overimposing over the long-lasting emergent signal produced by the debris flow (Figures 3a and 3b). In the infrasound record such events appear as multiple blast waves grouping into signals of maximum duration of 20–30 s.

For the 29 May 2017 event, such transients are clearly detected with infrasound array processing starting 17:30 and are associated with back azimuth varying clockwise between 230 and 300° N and apparent velocity exceeding 400 m/s. The large azimuth variation and apparent velocity suggest moving sources at high altitude. Waveform characteristics (blast waves) and observed wave parameters (back azimuth and apparent velocity) suggest these transients are possibly produced by lightning activity.

In order to investigate the nature of these high-amplitude transients, we compared the infrasound observations with lightning occurrence detected by the World Wide Lightning Location Network (WWLLN), a globally distributed network of very low frequency receivers able to locate cloud-to-ground flashes on a global scale (Virts et al., 2013). Given the station density of the WWLLN, not all flashes are detected but only the strongest one. During the time of occurrence of the 29 May 2017 event (16:30–18:30 UTC), 17 flashes within a maximum distance of 30 km from the ILG array were detected by the WWLLN, produced within a thunderstorm moving clockwise south of the array (Figure A1a).

Figure A1 shows the time of occurrence of the flashes (lines in Figure A1b color coded for time) that is always followed by one transient in the infrasound data. However, not each single infrasound transient is preceded by a flash detected by the WWLLN, and this is likely related to the threshold of lightning location. Infrasound data following the 17 reported flashes are extracted and displayed in Figure A1c, showing how back azimuth evaluated from infrasound array analysis (colored circles in Figure A1c) is in good agreement with the real azimuth to the flash evaluated from the WWLLN event location (black diamond in Figure A1c). This confirms that the high-amplitude transients recorded both in the infrasound and seismic signals are related to a thundercloud and not to the debris flow event itself.

Appendix B: Infrasound Array Analysis

The array signal processing is based on the assumption that a signal is coherent at the different sensors, while noise does not show any correlation. In this study we applied a multichannel correlation method

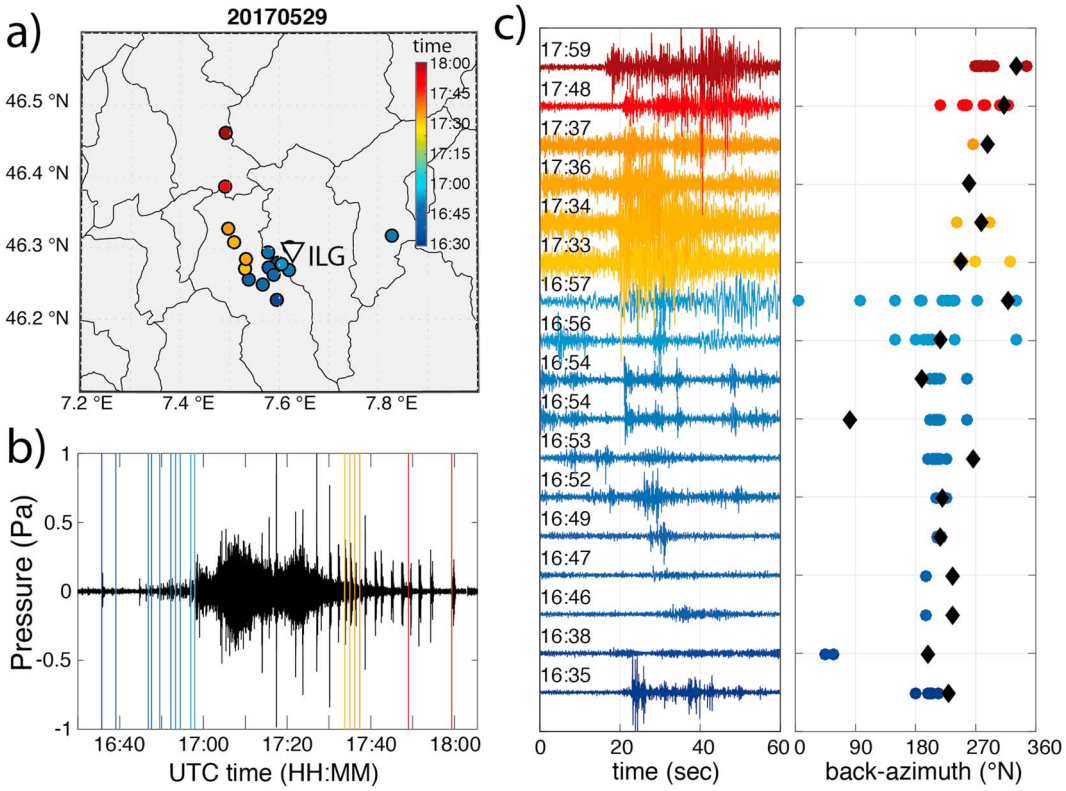

Figure A1. (a) Location of 17 flashes recorded by the World Wide Lightning Location Network in the time period 16:30–17:00 and 17:30–18:00 UTC of 29 May 2017 and within a distance of 30 km from the array. (b) Infrasound record of the debris flow with timing of the 17 detected flashes (vertical lines). All flashes are followed by a high-amplitude transient in the infrasound record. (c) The 60-second-long sample of infrasound data following the detected flashes showing the infrasound transient and corresponding back azimuth values as detected by the array (circles). Back azimuth evaluated from the flash location by World Wide Lightning Location Network (black diamond) is shown for comparison.

to identify signals from noise in terms of back azimuth (B_{az}) and apparent velocity (C_a) of the infrasonic ray propagating across the array and the corresponding time residual (Δt). The propagation back azimuth indicates the direction where the signal comes from and is related to the location of the source of the signal. The apparent velocity is the velocity the wave would travel if it was propagating in the same plane as defined by the array; it is related to the incident angle and thus the altitude of the source. The time residual is a parameter reflecting the degree of correlation of signal within the array and allows distinguishing signal from noise.

The signal processing procedure was performed on successive moving time windows (10 s in our case) on all possible triplets of sensors in the array. For an array with four sensors, there are four possible triplets. For each triplet of sensors, we performed cross-correlation analysis between signal recorded at two elements i and j of the triplet (Figure B1) and calculated the time delay (δt_{ij}) from the maximum value of the cross-correlation function. The time delays (δt_{ij}) are used to calculate the back azimuth (b_{az}) and apparent velocity (c_a) of a plane infrasound array crossing the array by solving the two equations:

$$\frac{L_{ij}\cos(\beta_{ij} - b_{az})}{\delta t_{ij}} = c_{ij}, \tag{B1}$$

$$\frac{L_{ik}\cos(\beta_{ik} - b_{az})}{\delta t_{ik}} = c_{ik}, \tag{B2}$$

where L_{ij} and β_{ij} are the distance and angle measured from north for the line segment between elements i and j of the array (Figure B1). By assuming a constant propagation velocity across the array ($c_{ij} = c_{ik} = c_a$), equations (B1) and (B2) can be solved to retrieve the propagation back azimuth (b_{az}) and apparent velocity (c_a) of the infrasound wave across the triplet.

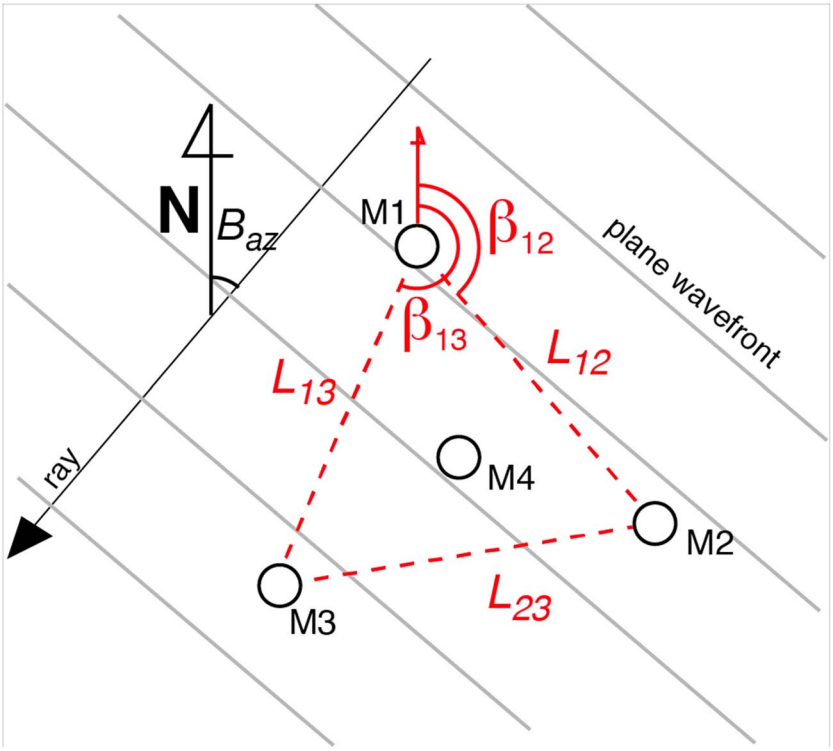

Figure B1. Sketch of a plane wavefield (gray lines) propagating across an array of four sensors (M1–M4, white circles) with a back azimuth (B_{az}). The red dashed line identifies a triplet of sensors, out of the four elements, used to evaluate (b_{az}) and apparent velocity (c_a), while L_{ij} and β_{ij} are the distance and angle between a couple of elements i and j of the array.

Considering the three pairs of station constituting each triplet the time residual (δt_n) is calculated as

$$\delta t_n = |\delta t_{ij} + \delta t_{jk} + \delta t_{ki}|. \tag{B3}$$

The time residual δt_n provides the degree of multichannel correlation across the triplet n. For highly correlated signals the time residual tends to 0 ($\delta t_n \rightarrow 0$), while it will be a positive value for uncorrelated signals.

The calculation of back azimuth (b_{az}), apparent velocity (c_a), and time residual (δt) is eventually performed for all the different triplets (N, four in our case) of sensors within the array, leading to a mean values of the time residual (Δt), infrasound back azimuth (B_{az}), and apparent velocity (C_a), as

$$\Delta t = \sum_{n=1}^{N} \frac{\delta t_n}{N} \quad n = 1, \ldots, N, \tag{B4}$$

$$B_{az} = \sum_{n=1}^{N} \frac{b_{az_n}}{N} \quad n = 1, \ldots, N, \tag{B5}$$

$$C_a = \sum_{n=1}^{N} \frac{c_{a_n}}{N} \quad n = 1, \ldots, N. \tag{B6}$$

When the Δt (equation (B4)) is below a given threshold value of time (0.1 s in our case), signal is detected within the time window of analysis (that corresponds to an infrasound detection), and it is fully characterized by its values of back azimuth (B_{az}) and apparent velocity (C_a). The latter can be eventually converted into the incident angle of the infrasonic ray (γ, i.e., angle between the ray and the normal to the plane) if the real sound propagation velocity (c) is known:

$$C_a = \frac{c}{\sin \gamma}. \tag{B7}$$

It is clear form equation (B7) that the apparent velocity (C_a) equals the sound propagation velocity (c) only for a wave propagating in the same plane defined by the array and will increase progressively as the incident angle decreases. For direct infrasound arrivals, higher-altitude sources will be characterized by higher values of the apparent propagation velocity.

Acknowledgments
The authors comply with AGU's data policy and infrasound detections resulting from array processing and used to achieve all the findings and create all the figures are freely available in the Open Science Framework repository (https://osf.io/jv724). The authors are grateful to Giovanni Coco and three anonymous reviewers who provided useful and constructive reviews. The authors wish to thank the World Wide Lightning Location Network (http://wwlln.net), a collaboration among over 50 universities and institutions, for providing the lightning location data used in this paper. The research was performed in the framework of the m2a project funded by UNIFI. The salary of Fabian Walter was paid by the Swiss National Science Foundation (grant PP00P2_157551). The salary of Michaela Wenner was paid by the WSL CCAMM grant. Seismic installation and data handling were supported by the Swiss Seismological Service.

References

Allstadt, K. E., Matoza, R. S., Lockhart, A., Moran, S. C., Caplan-Auerbach, J., Haney, M., et al. (2018). Seismic and acoustic signatures of surficial mass movements at volcanoes. *Journal of Volcanology and Geothermal Research*, *264*, 76–106. https://doi.org/10.1016/j.volgeores.2018.09.007

Arattano, M., & Marchi, L. (2005). Measurements of debris flow velocity through cross-correlation of instrumentation data. *Natural Hazards and Earth System Sciences*, *5*, 137–142. https://doi.org/10.5194/nhess-5-137-2005

Badoux, A., Graf, C., Rhyner, J., Kuntner, R., & McArdell, B. W. (2009). A debris-flow alarm system for the Alpine Illgraben catchment: Design and performance. *Natural Hazards*, *49*, 517–539.

Barfucci, G., & Ripepe, M. (2018). Dome collapse interaction with the atmosphere. *Geophysical Research Letters*, *45*, 8923–8930. https://doi.org/10.1029/2018GL078243

Bennett, G. L., Molnar, P., McArdell, B. W., Schlunegger, F., & Burlando, P. (2013). Patterns and controls of sediment production, transfer and yield in the Illgraben. *Geomorphology*, *188*, 68–82. https://doi.org/10.1016/j.geomorph.2012.11.029

Berger, C., McArdell, B. W., & Schlunegger, F. (2011). Direct measurement of channel erosion by debris flows, Illgraben, Switzerland. *Journal of Geophysical Research*, *116*, F01002. https://doi.org/10.1029/2010JF001722

Bowman, J. R., Baker, G. E., & Bahavar, M. (2005). Ambient infrasound noise. *Geophysical Research Letters*, *32*, L09803. https://doi.org/10.1029/2005GL022486

Burtin, A., Bollinger, L., Vergne, J., Cattin, R., & Nabelek, J. (2008). Spectral analysis of seismic noise induced by rivers: A new tool to monitor spatiotemporal changes in stream hydrodynamics. *Journal of Geophysical Research*, *113*, B05301. https://doi.org/10.1029/2007JB005034

Chou, H. T., Chang, Y. L., & Zhang, S. C. (2013). Acoustic signals and geophone response of rainfall-induced debris flows. *Journal of the Chinese Institute of Engineers*, *36*(3), 335–347.

Delle Donne, D., Ripepe, M., De Angelis, S., Cole, P. D., Lacanna, G., Poggi, P., & Stewart, R. (2014). Thermal, acoustic and seismic signals from pyroclastic density currents and Vulcanian explosions at SoufriÃÍre Hills Volcano, Montserrat. *Geological Society, London, Memoires*, *39*, 169–178. https://doi.org/10.1144/M39.9

Evers, L. G., & Haak, H. W. (2001). Listening to sounds from an exploding meteor and oceanic waves. *Geophysical Research Letters*, *28*(1), 41–44.

Feng, H. N., Yang, Y. C., Chunchuzov, I., & Teng, P. X. (2014). Study of infrasound from a water dam. *Acta Acustica*, *100*, 1–9. https://doi.org/10.3813/AAA918702

Gimbert, F., Tsai, V. C., & Lamb, M. P. (2014). A physical model for seismic noise generation by turbulent flow in rivers. *Journal of Geophysical Research: Earth Surface*, *119*, 2209–2238. https://doi.org/10.1002/2014JF003201

Hubl, J., Schimmel, A., Kogelnig, A., Suriñach, E., Vilajosana, I., & McArdell, B. W. (2013). A review on acoustic monitoring of debris flow. *International Journal of Safety and Security Engineering*, *3*(2), 105–115.

Hurlimann, M., Rickenmann, D., & Graf, C. (2003). Field and monitoring data of debris-flow events in the Swiss Alps. *Canadian Geotechnical Journal*, *40*, 161–175. https://doi.org/10.1139/t02-087

Johnson, J. B., & Palma, J. L. (2015). Lahar infrasound associated with Volcan Villarrica's 3 March 2015 eruption. *Geophysical Research Letters*, *42*, 6324–6331. https://doi.org/10.1002/2015GL065024

Kean, J. W., Coe, J. A., Coviello, V., Smith, J. B., McCoy, S. W., & Arattano, M. (2015). Estimating rates of debris flow entrainment from ground vibrations. *Geophysical Research Letters*, *42*, 6365–6372. https://doi.org/10.1002/2015GL064811

Kogelnig, A., Hubl, J., Suriñach, E., Vilajosana, I., & McArdell, B. W. (2014). Infrasound produced by debris flow: Propagation and frequency content evolution. *Natural Hazards*, *70*(3), 1713–1733.

Kogelnig, A., Suriñach, E., Vilajosana, I., Hübl, J., Sovilla, B., Hiller, M., & Dufour, F. (2011). On the complementariness of infrasound and seismic sensors for monitoring snow avalanches. *Natural Hazards and Earth System Sciences*, *11*(8), 2355–2370.

Kudo, N. (1993). Control of infrasonic noise from waterfall. *Journal of Low Frequency Noise, Vibration and Active Control*, *12*, 149–155. https://doi.org/10.1177/026309239301200404

Lacanna, G., Ichihara, M., Iwakuni, M., Takeo, M., Iguchi, M., & Ripepe, M. (2014). Influence of atmospheric structure and topography on infrasonic wave propagation. *Journal of Geophysical Research: Solid Earth*, *119*, 2988–3005. https://doi.org/10.1002/2013JB010827

Lacanna, G., & Ripepe, M. (2013). Influence of near-source volcano topography on the acoustic wavefield and implication for source modeling. *Journal of Volcanology and Geothermal Research*, *250*, 9–18. https://doi.org/10.1016/j.jvolgeores.20102.10.005

Lai, V. H., Tsai, V. C., Lamb, M. P., Ulizio, T. P., & Beer, A. R. (2018). The seismic signature of debris flows: Flow mechanics and early warning at Montecito, California. *Geophysical Research Letters*, *45*, 5528–5535. https://doi.org/10.1029/2018GL077683

Li, C. A., Hu, X. W., & Wang, L. W. (2012). Infrasound monitoring and early warning of debris flow along montanic railway line. *Technical Acoustics/Shengxue Jishu*, *31*(4), 351–356.

Liu, D. L., Leng, X. P., Wei, F. Q., Zhang, S. J., & Hong, Y. (2015). Monitoring and recognition of debris flow infrasonic signals. *Journal of Mountain Science*, *12*(4), 797–815.

Marchetti, E., Ripepe, M., Ulivieri, G., & Kogelnig, A. (2015). Infrasound array criteria for automatic detection and front velocity estimation of snow avalanches: Towards a real-time early-warning system. *Natural Hazards and Earth System Sciences*, *15*, 2545–2555. https://doi.org/10.5194/nhess-15-2545-2015

McArdell, B. W., Bartelt, P., & Kowalski, J. (2007). Field observations of basal forces and fluid pore pressure in a debris flow. *Geophysical Research Letters*, *34*, L07406. https://doi.org/10.1029/2006GL029183

Preiswerk, L. E., Walter, F., Anandakrishnan, S., Barfucci, G., Beutel, J., Burkett, P. G., et al. (2016). Monitoring unstable parts in the ice-covered Weissmies northwest face. In *In 13th Congress Interpraevent 2016* (pp. 434–443). https://doi.org/10.3929/ethz-a-010811690

Rickenmann, D., Hülimann, M., Graf, C., Näf, D., & Weber, D. (2001). Murgang-beobachtungsstationen in der Schweiz. *Wasser Energie Luft*, *93*(1/2), 1–8.

Ripepe, M., De Angelis, S., Lacanna, G., & Voight, B. (2010). Observation of infrasonic and gravity waves at Soufirere Hills Volcano, Montserrat. *Geophysical Research Letters*, *37*, L00E14. https://doi.org/10.1029/2010GL042557

Rost, S., & Thomas, C. (2002). Array seismology: Methods and applications. *Reviews of Geophysics*, *40*(3), 1008. https://doi.org/10.1029/2000RG000100

Schimmel, A., & Hübl, J. (2016). Automatic detection of debris flows and debris floods based on a combination of infrasound and seismic signals. *Landslides*, *13*(5), 1181–1196.

Schimmel, A., Hübl, J., McArdell, B. W., & Walter, F. (2018). Automatic identification of alpine mass movements by a combination of seismic and infrasound sensors. *Sensors*, *18*(5), 1658. https://doi.org/10.3390/s18051658

Schlunegger, F., Badoux, A., McArdell, B. W., Gwerder, C., Schnydrig, D., Rieke-Zapp, D., & Molnar, P. (2009). Limits of sediment transfer in an alpine debris-flow catchment, Illgraben, Switzerland. *Quaternary Science Reviews*, *28*, 1097–1105.

Schmandt, B., Aster, R. C., Scherler, D., Tsai, V. C., & Karlstrom, K. (2013). Multiple fluvial processes detected by riverside seismic and infrasound monitoring of a controlled flood in the Grand Canyon. *Geophysical Research Letters*, *40*, 4858–4863. https://doi.org/10.1002/grl.50953

Scott, E. D., Hayward, C. T., Kubichek, R. F., Hamann, J. C., Pierre, J. W., Comey, B., & Mendenhall, T. (2007). Single and multiple sensor identification of avalanche-generated infrasound. *Cold Regions Science and Technology*, *47*(1), 159–170.

Szuberla, C. A., & Olson, J. V. (2004). Uncertainties associated with parameter estimation in atmospheric infrasound arrays. *The Journal of the Acoustical Society of America*, *115*(1), 253–258.

Tsai, V. C., Minchew, B., Lamb, M. P., & Ampuero, J.-P. (2012). A physical model for seismic wave generation from sediment transport in rivers. *Geophysical Research Letters*, *39*, L02404. https://doi.org/10.1029/2011GL050255

Ulivieri, G., Marchetti, E., Ripepe, M., Chiambretti, I., De Rosa, G., & Segor, V. (2011). Monitoring snow avalanches in Northwestern Italian Alps using an infrasound array. *Cold Regions Science and Technology*, *69*(2), 177–183.

Virts, K. S., Wallace, J. M., Hutchins, M. L., & Holzworth, R. H. (2013). A new ground-based, hourly global lightning climatology. *BAMS*, 1831–1891. https://doi.org/10.1175/BAMS-D-12-00082

Walter, F., Burtin, A., McArdell, B. W., Hovius, N., Weder, B., & Turowski, J. M. (2017). Testing seismic amplitude source localization for fast debris-flow detection at Illgraben, Switzerland. *Natural Hazards and Earth System Sciences*, *17*, 935–955. https://doi.org/10.5194/nhess-17-939-2017